

Kinetic and Mechanistic Study on *p*-Quinodimethane Formation in the Sulfinyl Precursor Route for the Polymerization of Poly(*p*-phenylenevinylene) (PPV)

Laura Hermosilla,^{†,‡} Saron Catak,^{†,‡} Veronique Van Speybroeck,^{*,†,‡} and Michel Waroquier^{†,‡}

[†]Center for Molecular Modeling, Ghent University, Technologiepark 903, B9052 Zwijnaarde, Belgium, and

[‡]QCM-Alliance Ghent-Brussels, Belgium

Joke Vandenbergh,[§] Filip Motmans,^{§,⊥} Peter Adriaenssens,[§] Laurence Lutsen,^{||} Thomas Cleij,[§] and Dirk Vanderzande^{*,§,||}

[§]Hasselt University, Campus Diepenbeek, Institute for Materials Research, Agoralaan Building D, 3590 Diepenbeek, Belgium, and ^{||}IMEC-IMOMEC, Wetenschapspark 1, 3590 Diepenbeek, Belgium.

[⊥]Current address: VITO, Boeretang 200, 2400 MOL, Belgium

Received June 12, 2010; Revised Manuscript Received June 28, 2010

ABSTRACT: The kinetics of *p*-quinodimethane formation in the sulfinyl precursor route for the poly(*p*-phenylenevinylene) (PPV) polymerization was studied using stop-flow UV–vis spectroscopy and theoretical first principle calculations. Different sulfinyl monomers were studied by means of quantitative kinetic experiments regarding the *p*-quinodimethane formation in 2-butanol. The influence of the solvent, the nature of the aromatic moiety, and the substituents on the phenyl core was analyzed by means of qualitative experiments. Quantitative measurements, using pseudo-first-order reaction conditions, were performed in order to assess the effect of the polarizer and the leaving group on the reaction rates. To obtain additional fundamental insight into the pathway leading to *p*-quinodimethane formation, density functional theory calculations were performed and subsequent reaction rate coefficients were determined from a theoretical point of view, enabling a profound comparison with experiment. From all these data, an E₂ mechanism is proposed for the *p*-quinodimethane formation in the sulfinyl precursor route.

Introduction

The synthesis and characterization of conjugated polymers has been a topic of broad interest in the past few decades.¹ Among these conjugated materials, poly(*p*-phenylenevinylene) (PPV) gained a lot of interest due to its luminescent behavior as discovered by Burroughes and co-workers.² PPV and its derivatives can be synthesized using several approaches, but usually a precursor route toward PPV is used yielding a soluble precursor polymer that can then be converted to the conjugated structure through an additional (thermal) conversion step. Generally, five precursor routes are well described: the Wessling,³ the Gilch,⁴ the sulfinyl,⁵ the xanthate,⁶ and the dithiocarbamate⁷ route. These routes all have in common the formation of the precursor polymer, which is achieved through polymerization of a *p*-quinodimethane system that is produced through a base-induced treatment of a *p*-xylene derivative. For the Wessling precursor route, Cho and co-workers intensively studied the *p*-quinodimethane formation and polymerization behavior.⁸ For the *p*-quinodimethane formation, a reversible E_{1cb} mechanism was suggested, where deprotonation to yield a carbanion is a reversible step and the expulsion of the leaving group is the rate-determining step in the elimination reaction.

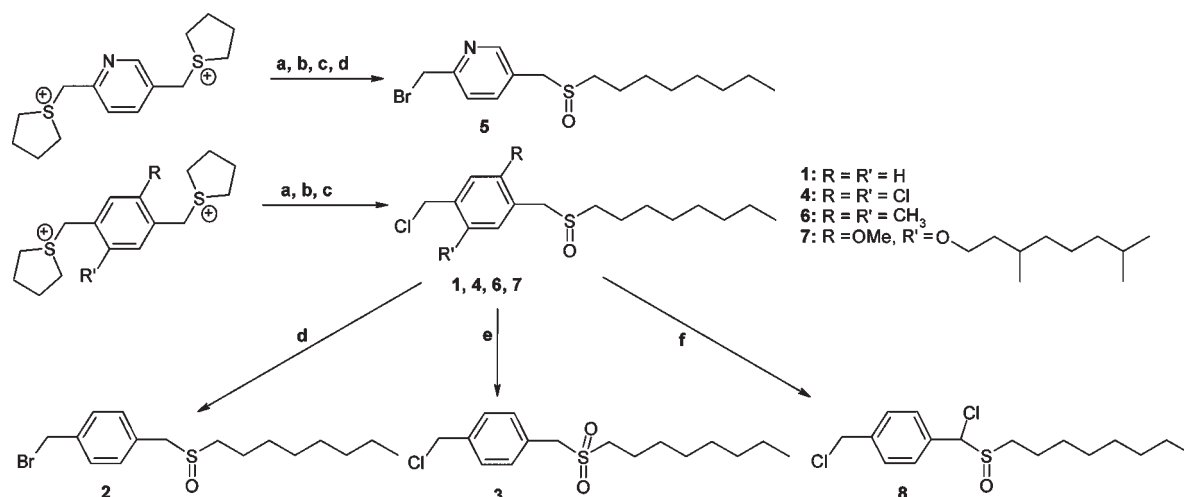
In our view, kinetic data on *p*-quinodimethane formation can be of major interest to predict the outcome of copolymerization reactions involving two different *p*-quinodimethane systems. For

this purpose, we performed a set of qualitative kinetic measurements using *in situ* UV–vis spectroscopy on several sulfinyl-derived monomers (Scheme 1, monomers 1–8) in 2-butanol. This solvent seems to be excellent to obtain high molecular weight PPV precursor polymers in high yield as discovered by some of the authors a few years ago.⁹ For comparative purposes, additional quantitative kinetic experiments were performed on monomers 1–3 (Scheme 1) which differ in the leaving or/and polarizer groups. These kinetic data provided insight into mechanistic details, which were further validated by computational methods. Theoretical calculations based on first principles form an ideal tool to obtain more fundamental insight into reaction mechanisms; they allow the calculation of intermediates, which are short-lived and not isolated in experiments. Base-induced reaction rate coefficients of monomers 1–3 leading to the *p*-quinodimethane intermediates were predicted by use of the transition state theory, and results were compared with experimental data from the quantitative measurements. The effect of solvent on the reaction rate coefficient was also discussed in detail. On the basis of theoretical calculations, a reaction mechanism is proposed for the *p*-quinodimethane formation in the sulfinyl precursor route for PPV polymerization.

Experimental Section

All chemicals were purchased from Aldrich or Acros and used without further purification unless stated otherwise. The required monomers 1–8 are synthesized according to the procedure developed in our research group and are described elsewhere.^{10,11} However, a general scheme is depicted in Scheme 1.

*Corresponding authors. E-mail: veronique.vanspeybroeck@ugent.be (V.V.S.); dirk.vanderzande@uhasselt.be (D.V.).

Scheme 1. Synthesis of the Required Monomers^a

^a Reaction conditions: (a) Na-*t*BuO, *n*-octanethiol, MeOH; (b) *n*-octane; (c) H₂O₂/TeO₂, HCl, MeOH; (d) LiBr (10 equiv), 3-pentanone, reflux; (e) *m*-CPBA, CH₂Cl₂; (f) *N*-chlorosuccinimide, CH₂Cl₂, pyridine.

In situ UV–vis measurements were performed on a Cary 500 UV–vis–NIR spectrophotometer equipped with a stop-flow module supplied by Hi-Tech Limited, containing a sample cell with a 10 mm path length (detail of the experimental set-up for the UV-vis stop flow accessory is provided in Supporting Information). “Scanning kinetics” and “Kinetics” software supplied by Varian is used to investigate the regions or wavelengths of interest. Monomer solutions were prepared by dissolving an amount of monomer in 2-butanol to obtain a 10^{−4} M solution. Base solutions were prepared from a 10^{−2} M sodium *tert*-butoxide stock solution in 2-butanol. Both monomer and base solution were degassed with nitrogen prior to the kinetic run, and the reaction temperature was maintained at 298 K. For the quantitative measurements computational nonlinear least-squares fitting was performed using the program Kaleidagraph.

Computational Details

Computational calculations based on first principles are an ideal tool for the prediction of properties that are not accessible experimentally, as is the case for the highly unstable carbanion intermediate involved in the reaction under study.

All ab initio computations were performed with the Gaussian 03 software package.¹² Some of the initial geometries were generated by an in-house developed software, the program Zeobuilder.¹³ Density functional theory (DFT) methods have been shown to be more efficient than wave function based procedures such as highly correlated post-Hartree–Fock methods due to their excellent cost to performance ratio. The B3LYP/6-31+G(d,p) level of theory was used for geometry optimizations. This functional is known for its ability to produce good geometries.^{14,15} The 6-31+G(d,p) double- ζ basis set comprises polarization functions on all atoms for a good description of the hydrogen bonds.¹⁶ Harmonic vibrational frequencies were computed at the same level of theory as the geometry optimization and used to provide zero-point vibrational energy (ZPVE) and to confirm the nature of the stationary points. In a second step, the MPW1K¹⁷ functional was employed with the same basis set to refine energies. This functional is especially developed for kinetics and is expected to give reliable results. Our main objective in this study is the prediction of qualitative trends that might contribute to a better understanding of the experimental results, and therefore the proposed functional is well suited. Nevertheless, the influence of the level of theory on rate constants is also investigated by comparison to experimental data. The following methods are used: MPWB1K,^{18–20} MPW1B95,²⁰ PBE0,²¹ BMK,²²

and MP2,²³ combined with these basis sets: 6-31++G(d,p), 6-311+G(3df,2p), and cc-pV(T+d)Z+.²⁴ Energies were corrected by adding the corresponding ZPVE scaled by a factor of 0.9806.²⁵ Caution is needed in interpreting the quantitative values for the barriers resulting from DFT calculations, as the absolute values for the energies might vary largely depending on the specific functional that is used.²⁶

The base-induced reaction rate coefficients of monomers 1–3 leading to the *p*-quinodimethane intermediates were predicted on the basis of transition state theory (TST),²⁷ using expression 1, which is complemented in the in-house developed software code TAMkin²⁸

$$k(T) = \frac{k_B T}{h} (c^0)^{1-m} \frac{q_{TS}}{\prod q_R} \exp\left(\frac{-\Delta E_0}{k_B T}\right) \quad (1)$$

where k_B is Boltzmann’s constant, T is the temperature, h is Planck’s constant, c^0 is the standard unit of concentration, m is the molecularity of the reaction, q_R and q_{TS} relate to the molecular partition functions of the reactants and transition state, respectively, and ΔE_0 is the ZPVE-corrected energy difference between the TS and the reactants (i.e., the reaction barrier) at 0 K.

The effect of the solvent is explicitly taken into account by surrounding the reactive centers with explicit alcohol molecules. In recent years, several approaches have become popular for studying reactions in solution, including the use of implicit/explicit solvation.^{29–32} In these mixed models, solvation is simulated by the addition of one or more explicit solvent molecules, followed by embedding the structure in a polarizable medium characterized by a fixed dielectric constant to take into account the electrostatic effect of the solvent dielectricum. However, recent publications show that explicit solvation alone can give rise to reliable results provided that the number and position of the solvent molecules are correctly selected.^{32,33} Bearing this in mind, a detailed analysis was performed to obtain the optimum number of coordinating solvent molecules. Geometry optimizations, prediction of the rate constants, etc., were carried out on the “solvated system”.

Results and Discussion

Experimental Results. It is generally known that *p*-quinodimethane systems show a typical absorption band around 320 nm in the UV–vis spectrum. The exact maximum wavelength depends on the substituents on the aromatic

moiety. Hence, this technique is an excellent tool in providing kinetic data through continuous monitoring of this specific signal. Upon addition of an excess of a base solution (Na-tBuO) to a 10^{-4} M solution of a sulfinyl monomer in 2-butanol, a typical plot is observed using stop-flow UV-vis spectroscopy. An example of such a plot is depicted in Figure 1. Three important signals become clear. At 226 nm the monomer signal is constantly decreasing during the kinetic run. At 313 nm the *p*-quinodimethane signal shows a fast increase followed by a somewhat slower decrease. At 260 nm a third signal becomes clear which is assigned to the solvent substituted product as was proven using mass spectroscopy. At 290 nm a clean isosbestic point shows that solvent substitution occurs at the *p*-quinodimethane stage of the reaction. No indications for polymer formation during the kinetic runs were found probably due to the very low

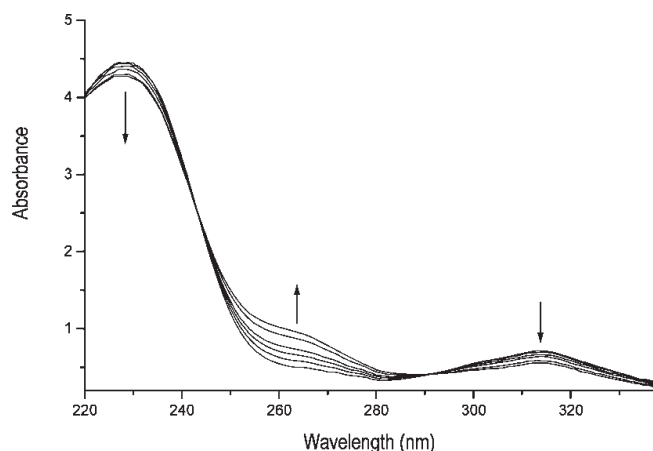


Figure 1. UV-vis spectra for *p*-quinodimethane formation and subsequent solvent substitution for a few selected times.

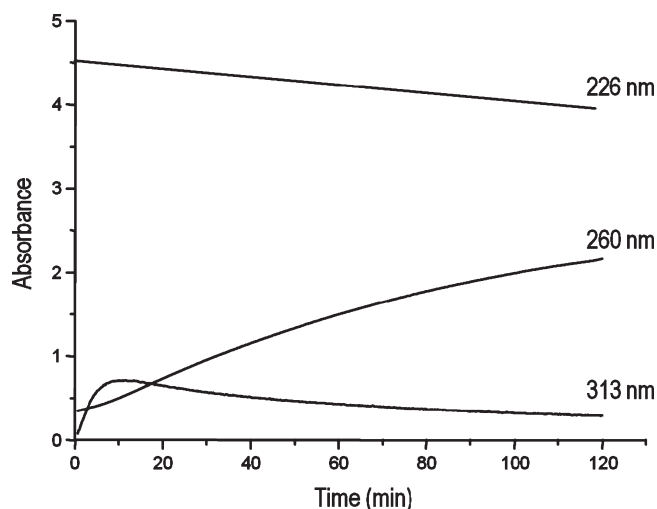


Figure 2. Absorption at 226, 260, and 313 nm versus time.

concentrations of the *p*-quinodimethane system, which precludes initiation of polymerization, since the initiating species is believed to be formed through dimerization of two *p*-quinodimethane systems. A plot of the three signals as a function of time is depicted in Figure 2.

The general reaction scheme for *p*-quinodimethane formation and subsequent consumption is depicted in Scheme 2. Basic treatment of monomers **1–8** yields a *p*-quinodimethane system that is consumed to give the solvent substituted product. 2-Butanol was used as the solvent for the kinetic measurements because this solvent has proven to be very suitable to yield different precursor polymers in a high yield and with high molecular weights. In Figure 3, normalized *p*-quinodimethane absorption of monomer **1** versus the reaction time is depicted as a function of increasing base concentrations.

A set of qualitative measurements on substituted or heteroaromatic derivatives **1–8** was performed in 2-butanol. The relative rate of the *p*-quinodimethane formation was determined from the time when the maximum absorbance of the *p*-quinodimethane signal was reached (t_{max}). The same base concentration was used for all measurements. From the listed t_{max} values (Table 1) some general conclusions can be drawn. Altering the leaving group from chlorine to bromine does not affect the reaction rate significantly. However, when the sulfinyl polarizer is replaced by a sulfonyl function, t_{max} decreases from 77 to 5.5 s, indicating that the acidity of the methylene protons next to the polarizer has a major impact on the reaction rate. Electron-withdrawing substituents on the phenyl moiety of monomer **4** increase the reaction rate drastically since the maximum absorbance is already reached after only 1.5 s (Figure 4). Also, the rate of the pyridine-derived monomer **5** ($t_{\text{max}} = 8$ s) was much higher than the normal PPV monomer **2**. Besides the decrease in the $\text{p}K_{\text{a}}$ of the benzylic protons due to the electron-withdrawing

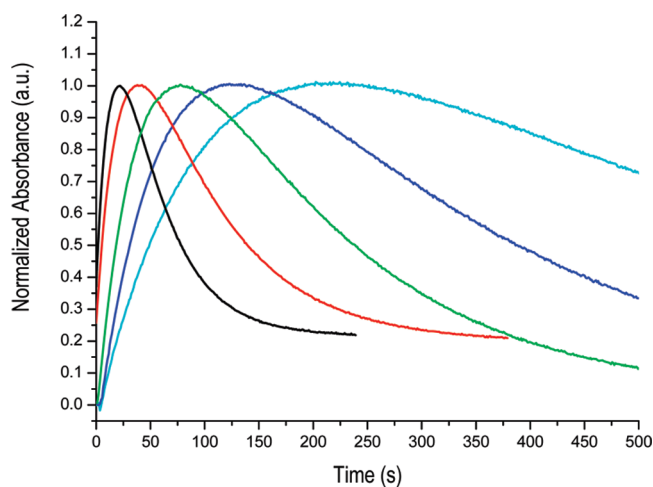


Figure 3. Normalized absorption at 313 nm versus time for monomer **1** as a function of increasing base concentration (increasing base concentration from cyan to black).

Scheme 2. General Reaction Scheme of *p*-Quinodimethane Formation and Solvent Substitution in the Sulfinyl Precursor Route

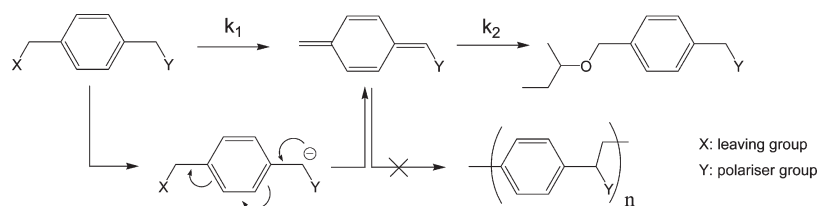
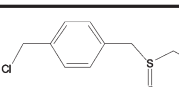
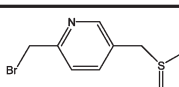
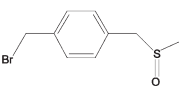
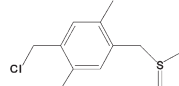
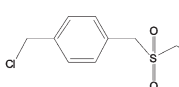
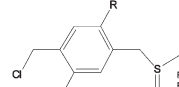
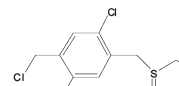
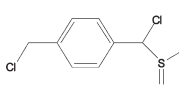


Table 1. Values of t_{\max} for Monomers 1–8

Monomer	t_{\max} (s)	Monomer	t_{\max} (s)
1 	77	5 	8
2 	69	6 	211
3 	5.5	7 	252
4 	1.5	8 	1.4

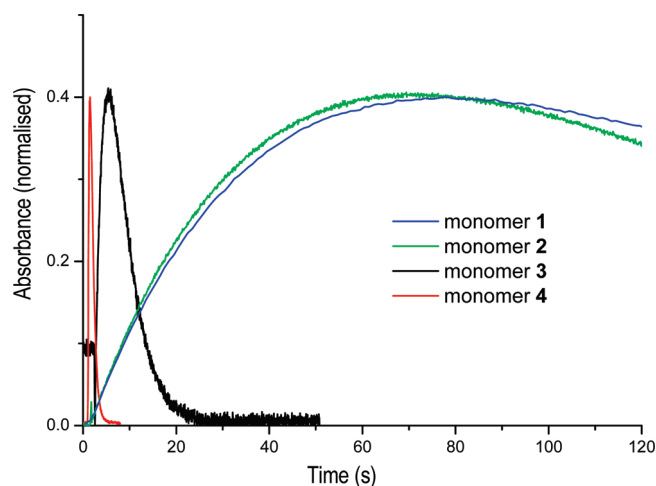


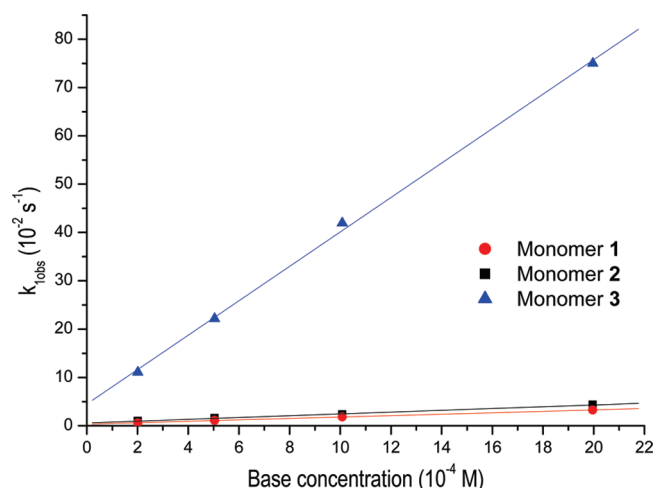
Figure 4. Absorption at 313 nm versus time for monomers 1–4.

Table 2. Overview of the Observed Pseudo-First-Order Rate Coefficient k_{obs} for Monomers 1–3 as a Function of the *tert*-Butoxide Base Concentration at 298 K

[base] (10^{-4} M)	k_{obs} (10^{-2} s $^{-1}$)		
	monomer 1	monomer 2	monomer 3
2.02	0.571 ± 0.027	0.961 ± 0.018	11.039 ± 0.706
5.04	1.107 ± 0.041	1.588 ± 0.058	22.162 ± 2.655
10.08	1.815 ± 0.024	2.340 ± 0.124	41.949 ± 3.301
20.17	3.258 ± 0.296	4.343 ± 0.314	75.661 ± 4.669

nitrogen atom, the rate increase of monomer 5 can also be attributed to the somewhat lower resonance energy of the pyridine unit compared to the phenyl moiety. Furthermore, the reaction rate decreases significantly when electron-donating substituents like methyl (6) or alkoxy (7) groups are implanted on the phenyl core. The maximum absorbance of both *p*-quinodimethane systems is only reached after more than 200 s. The implementation of a chlorine atom on the benzylic carbon next to the sulfinyl function in monomer 8 also strongly increases the acidity of the geminate proton, which is reflected in a low value of t_{\max} , comparable to that of monomer 4.

To obtain more detailed information on the *p*-quinodimethane formation, some additional quantitative experiments were performed. When using a large excess of base

Figure 5. Plot of the observed pseudo-first-order rate coefficient k_{obs} at 298 K versus the *tert*-butoxide base concentration.

versus monomer, pseudo-first-order reaction conditions are created, and the kinetic data obtained from the UV–vis measurements can be fitted using a kinetic model for a consecutive first-order reaction according to eq 2.³⁴ In this way, some quantitative data were obtained. For this part of the study, we analyzed the influence of the leaving group and the polarizer on the reaction rate coefficient by performing several experiments on monomers 1–3.

$$\text{Abs}_{313} = a(e^{-k_{\text{obs}}t} - e^{-k_{2\text{obs}}t}) + b \quad (2)$$

In the fit equation, Abs_{313} is the absorption at 313 nm, a and b are constant values, k_{obs} and $k_{2\text{obs}}$ are the observed pseudo-first-order rate coefficients for *p*-quinodimethane formation and solvent substitution, respectively, and t is the reaction time.

Excellent correlation coefficients (>0.999) are obtained, and each measurement is repeated three times to ensure good reproducibility. In Table 2, the observed pseudo-first-order rate constants k_{obs} are summarized for monomers 1–3. Plotting these values versus the applied base concentrations yields a straight line with good correlation coefficients in every case (Figure 5). The slope of the straight lines corresponds to the absolute rate constant k_1 of the *p*-quinodimethane formation. The values of k_1 are summarized in

Table 3. k_1 Values for Monomers 1–3 at 298 K

	k_1 (L mol ⁻¹ s ⁻¹)	R^2 ^a
monomer 1	14.62 ± 0.36	0.9994
monomer 2	18.44 ± 0.68	0.9986
monomer 3	356.08 ± 9.37	0.9993

^a R represents the correlation coefficient.

Table 3. As shown in that table, the rate coefficient of *p*-quinodimethane formation increases significantly when the sulfinyl polarizer group (monomer 1) is replaced by a sulfonyl group (monomer 3). Apparently, the pK_a value of the benzylic proton largely influences the reaction rate. A lower pK_a value, indicating higher acidity, correlates well with a higher rate constant. On the other hand, the reaction rate is not affected significantly upon changing the leaving group from chlorine to bromine. This indicates that the expulsion of the leaving group is a fast process. However, it is not clear whether proton abstraction and halide expulsion are coupled and whether the reaction occurs in a concerted fashion or through a stepwise mechanism involving a carbanion intermediate. This point will be further discussed in the Computational section. Nonetheless, experimental findings show that all factors stabilizing the formation of a carbanion, such as electron-withdrawing groups on the phenyl core or on the benzylic carbon as well as an electron-poor heteroaromatic core, will increase *p*-quinodimethane formation rate. On the contrary, electron-donating groups on the phenyl core or electron-rich monomers in general will have a negative effect on the reaction rate. However, it is not possible to state with certainty that the mechanism by which *p*-quinodimethane formation takes place from a sulfinyl monomer follows an irreversible E_{1cb} or a concerted E_2 mechanism. The nature of the elimination reaction will have a major influence on the outcome of copolymerization reactions. If the rates of *p*-quinodimethane formation of different monomers are not of the same order of magnitude, mixtures of homopolymers will be obtained instead of random copolymers.

Ab Initio Calculation Results. *Rate Coefficients.* Geometry optimizations of the transition states corresponding to the reactions of monomers 1–3 were carried out at the B3LYP/6-31+G(d,p) level of theory. Afterward, internal reaction coordinate (IRC) calculations were performed in order to find the reactants and products structures that are connected by each transition state. All the optimizations were followed by a normal-mode analysis to ensure that the calculated structures are either a local minimum or a transition state (0 or 1 imaginary frequency, respectively). The B3LYP/6-31+G(d,p) combination has been extensively proven to be suitable for obtaining good geometries for stationary points but is known to have a general tendency to underestimate reaction barriers.³⁵ MPW1K, developed especially for kinetic applications, performs better, so a subsequent energy calculation with MPW1K/6-31+G(d,p) was carried out on the optimized structures.

As a first approximation, calculations were performed *in vacuo*, considering only the two reactants, that is, the monomer and the *tert*-butoxide anion responsible for the deprotonation. An equilibrium between the *tert*-butoxide and the 2-butanol solvent is expected in the reaction medium, leading to the formation of *sec*-butoxide anions, which could also act as base. Thus, both possible bases, *tert*-butoxide and *sec*-butoxide, have been taken into consideration in the calculations. The optimized geometry is sensitive to the input structure, since the conventional optimization method employed is based on the gradient in energy and can only locate

local minima. Therefore, different initial positions of the reactants were checked to ensure that the global minimum is encountered. Optimized structures of reactants, transition states, and products for the reactions corresponding to monomers 1 and 3 with *tert*-butoxide as base are depicted in Figure 6 (xyz coordinates provided in the Supporting Information). The molecular structure of monomer 2 differs from 1 only by the identity of the halogen atom in the leaving group and is therefore not depicted. Additionally, no significant differences in reactions rate coefficients were found for the case of *sec*-butoxide as base. Crucial geometrical parameters for all three monomers are listed in Table 4. While monomers 1 and 2 have similar breaking and forming bond lengths, monomer 3 presents moderately different distances, which is consistent with the difference in rate constants. Geometries of the resulting products illustrate that the halide is still bonded to the benzylic carbon, which seems to correspond to the carbanion intermediate that is expected for a stepwise process. However, a closer look at the product structures reveals that the halogen–carbon bonds are elongated and the planarity at the deprotonated carbon is not typical for a carbanion. These geometrical factors point toward a concerted process rather than a stepwise one, although gas-phase results are not conclusive enough to differentiate unequivocally between them. The inclusion of the solvent effect is necessary to correctly model this process and to unravel the mechanism; this will be further discussed in detail.

The values for the reaction rate coefficients were calculated according to eq 1 between 200 and 400 K (experimental data determined at 298 K). Thereafter, kinetic parameters were estimated by fitting the Arrhenius equation to these data. The rate constants at 298 K obtained for the proton abstraction reaction of monomers 1, 2, and 3 by the *tert*-butoxide anion show the experimentally observed trend, as can be confirmed from data given in Table 5, where all the kinetic parameters are tabulated, i.e., preexponential factor A , activation energy E_a , and rate constants $k_{1,i}$ ($k_{1,i}$ is the k_1 value for monomer i). The kinetic parameters predicted by the calculations with *sec*-butoxide as base are very similar to those obtained with *tert*-butoxide, so the rest of the discussion is centered on the latter. The theoretical ratios $k_{1,2}/k_{1,1}$ and $k_{1,3}/k_{1,1}$ are 2.9 and 16.9, respectively, whereas the corresponding experimental data are 1.3 and 24.4, respectively (Table 3). Although the ratios are relatively well reproduced, the quantitative absolute rate coefficients predicted by DFT calculations are several orders of magnitude higher than the experimental ones. As previously explained, our aim in this study is to obtain qualitative trends of the reaction rate constants, but even in that case, it is necessary to confirm that the computational method is suitable to describe the system at hand. Thus, estimations of the rate coefficients were repeated with a variety of more advanced electronic structure methods, in order to compare their performance to that of the one used so far, MPW1K/6-31+G(d,p). Single-point calculations were carried out on optimized structures using the following methods: MPWB1K, MPWB95, PBE0, BMK, and MP2. MPWB1K and MPWB95 are hybrid meta DFT methods developed for kinetics and thermochemistry, with good description of hydrogen bonding, weak van der Waals interaction, and partial bonding.^{20,36} PBE0 is a parameter free density functional model that gives adequate structural, thermodynamic, kinetic, and spectroscopic properties, which are not far from those delivered by the most reliable functionals that include heavy parametrization.²¹ The BMK functional is chosen because of its good performance for describing kinetics of

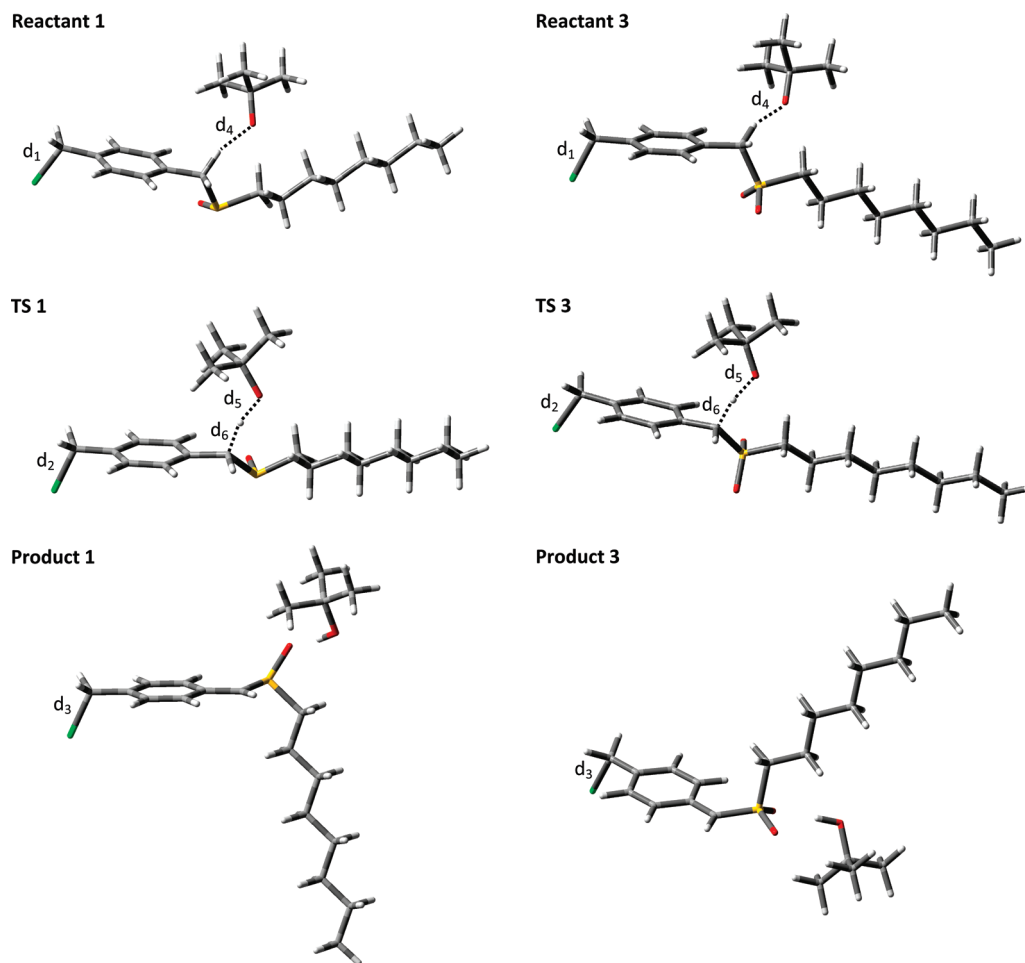


Figure 6. Schematic representation of the reactants, transition states, and products for the deprotonation reactions of monomers **1** (left) and **3** (right) by the *tert*-butoxide as base, optimized at B3LYP/6-31+G(d,p).

Table 4. Geometrical Parameters (Distances in Å) of Reactants and Transition States Corresponding to the Deprotonation of Monomers **1–3** with *tert*-Butoxide, Calculated at B3LYP/6-31+G(d,p) Level^a

monomer	d_1	d_2	d_3	d_4	d_5	d_6
1	1.87	1.90	1.99	1.90	1.32	1.32
2	2.03	2.07	2.33	1.89	1.33	1.31
3	1.86	1.88	1.97	1.84	1.36	1.29

^a See Figure 6 for definitions.

Table 5. Frequency Factors (A), Activation Energies (E_a), and Rate Coefficients ($k_{1,i}$) at 298 K, Corresponding to the Deprotonation of Monomers **1–3** with *tert*-Butoxide, Calculated at the MPW1K/6-31+G(d,p)//B3LYP/6-31+G(d,p) Level

monomer	A (L mol ⁻¹ s ⁻¹)	E_a (kJ mol ⁻¹)	$k_{1,i}$ (L mol ⁻¹ s ⁻¹)	$k_{1,i}/k_{1,1}$
1	1.16×10^{12}	14.0	4.16×10^9	1
2	2.07×10^{12}	12.7	1.21×10^{10}	2.9
3	2.44×10^{12}	8.8	7.02×10^{10}	16.9

reactions in general.^{37–39} The effect of higher order corrections is investigated with the MP2 second-order perturbation method. All these methods were combined with different basis sets, 6-31++G(d,p), cc-pV(T+d)Z+, and 6-311+G(3df,2p), in order to analyze its influence on the rate constants as well. The selection of the latter basis set was motivated by previous results that outline the difficulties associated with calculations on sulfur systems and conclude that the addition of high-exponent d and f polarization functions to the sulfur basis sets helps to reduce the error.^{40,41} One of the basis sets that has shown to provide good

performance in sulfur-containing systems is the 6-311+G(3df,2p),^{42–44} so we used it for the calculation of the rate coefficients in two ways: first, using it for all atoms and, second, employing a combined basis set consisting of the 6-31++G(d,p) for all atoms except sulfur, for which the larger 6-311+G(3df,2p) was considered. Henceforth, we will call this combined basis set 6-311+G(3df,2p)-S for simplicity. Another interesting basis set is the recently developed cc-pV(T+d)Z+, with tight d functions, that has provided barriers heights of many reactions very close to those of the larger aug-cc-pVTZ basis set, but with a much smaller cost, since the first has been designed by addition of only diffuse functions of low angular momentum on heavy atoms while the second one includes diffuse functions of both low and high angular momentum on all atoms.²⁴ The MP2 method was combined only with 6-31++G(d,p) and 6-311+G(3df,2p)-S basis sets. Because of the high computational cost of this methodology and on the basis of the results obtained with the rest of methods (see below), other basis sets were not used.

The values of the rate constants corresponding to the deprotonation reaction of monomers **1–3** calculated at different levels of theory are listed in Table 6. A general assessment of the results shows that the absolute values are several orders of magnitude higher than the experimental data, regardless of the combination of method and basis set employed. This is most likely due to the lack of a proper molecular environment in gas-phase calculations, which is expected to have an important influence, as will be explained

Table 6. Rate Coefficients ($\text{L mol}^{-1} \text{s}^{-1}$) at 298 K Corresponding to the Deprotonation of Monomers 1–3 with *tert*-Butoxide, Calculated at Different Levels of Theory

method	$k_{1,1}$	$k_{1,2}$	$k_{1,3}$	$k_{1,2}/k_{1,1}$	$k_{1,3}/k_{1,1}$
MPW1K/6-31+G(d,p)	4.16×10^9	1.21×10^{10}	7.02×10^{10}	2.9	16.9
MPW1K/6-31++G(d,p)	4.25×10^9	9.75×10^9	7.74×10^{10}	2.3	18.2
MPW1K/6-311+G(3df,2p)-S ^a	3.62×10^9	8.72×10^9	8.60×10^{10}	2.4	23.7
MPW1K/6-311+G(3df,2p)	1.74×10^9	3.75×10^9	4.54×10^{10}	2.2	26.1
MPW1K/cc-pV(T+d)Z+	2.77×10^{10}	6.09×10^{10}	8.15×10^{11}	2.2	29.5
B3LYP/6-31+G(d,p)	1.84×10^9	6.81×10^9	3.04×10^{10}	3.7	16.6
B3LYP/6-31++G(d,p)	1.87×10^9	4.77×10^9	3.44×10^{10}	2.6	18.4
B3LYP/6-311+G(3df,2p)-S	1.72×10^9	4.49×10^9	3.61×10^{10}	2.6	21.0
B3LYP/6-311+G(3df,2p)	6.52×10^8	2.28×10^9	1.97×10^{10}	3.5	30.2
B3LYP/cc-pV(T+d)Z+	8.93×10^9	2.21×10^{10}	3.33×10^{11}	2.5	37.3
MPWB1K/6-31++G(d,p)	9.40×10^8	2.45×10^9	5.73×10^{10}	2.6	61.0
MPWB1K/6-311+G(3df,2p)-S	8.61×10^8	2.27×10^9	6.77×10^{10}	2.6	78.6
MPWB1K/6-311+G(3df,2p)	3.92×10^8	1.15×10^9	3.24×10^{10}	2.9	82.6
MPWB1K/cc-pV(T+d)Z+	6.83×10^9	1.67×10^{10}	6.23×10^{11}	2.4	91.2
MPW1B95/6-31++G(d,p)	2.76×10^9	7.15×10^9	1.45×10^{11}	2.6	52.6
MPW1B95/6-311+G(3df,2p)-S	2.62×10^9	6.85×10^9	1.81×10^{11}	2.6	69.3
MPW1B95/6-311+G(3df,2p)	1.45×10^9	4.92×10^9	1.02×10^{11}	3.4	70.2
MPW1B95/cc-pV(T+d)Z+	2.10×10^{10}	5.11×10^{10}	1.70×10^{12}	2.4	81.0
PBE0/6-31++G(d,p)	3.31×10^{10}	7.58×10^{10}	5.42×10^{11}	2.3	16.4
PBE0/6-311+G(3df,2p)-S	3.02×10^{10}	6.92×10^{10}	6.49×10^{11}	2.3	21.4
PBE0/6-311+G(3df,2p)	1.31×10^{10}	3.74×10^{10}	2.73×10^{11}	3.0	20.8
PBE0/cc-pV(T+d)Z+	1.96×10^{11}	4.44×10^{11}	5.90×10^{12}	2.3	30.1
BMK/6-31++G(d,p)	9.31×10^8	2.00×10^9	1.99×10^{10}	2.1	21.4
BMK/6-311+G(3df,2p)-S	8.86×10^8	1.89×10^9	2.28×10^{10}	2.1	25.7
BMK/6-311+G(3df,2p)	5.51×10^8	1.60×10^9	1.43×10^{10}	2.9	25.9
BMK/cc-pV(T+d)Z+	5.96×10^9	1.37×10^{10}	1.69×10^{11}	2.3	28.4
MP2/6-31++G(d,p)	2.15×10^9	6.69×10^9	4.61×10^{10}	3.1	21.4
MP2/6-311+G(3df,2p)-S	2.94×10^9	8.92×10^9	7.55×10^{10}	3.0	25.7
experimental	14.62	18.44	356.08	1.3	24.4

^a The 6-311+G(3df,2p)-S basis set refers to the 6-31++G(d,p) with the extra 6-311+G(3df,2p) basis set in the sulfur atom.

extensively in the following section. Nevertheless, rather than focusing solely on the quantitative agreement between computed and experimental values, it is more important to validate whether qualitative trends are reproduced, so we focus our attention on the ratios $k_{1,2}/k_{1,1}$ and $k_{1,3}/k_{1,1}$. There is a general consistency in the estimation of the first ratio for all the combinations. Although always overestimated respect to the reference experimental data (1.3), the calculated values are within a relatively narrow range of 2.1–3.7. Larger differences are observed in the second ratio, where the selection of the method is crucial for obtaining good results. MPWB1K and MPW1B95 functionals with all four basis sets overestimate the ratio to a large extent, so neither of them should be used for this kind of calculations. Other methods provide values closer to the reference, although differences are observed depending on the choice of basis set. The smallest basis set 6-31+G(d,p) (only tested with MPW1K and B3LYP methods) gives rise to low ratios in both cases, modestly increased when the 6-31++G(d,p) basis set is used, highlighting the importance of the diffusion functions in the description of the sulfonyl group. The addition of *d* and *f* polarization functions to the sulfur atom through the 6-311+G(3df,2p) basis set improves the results significantly. However, the inclusion of these polarization functions on all the atoms does not perform so well and the values do not improve. The cc-pV(T+d)Z+ basis set overestimates the ratio with respect to the 6-311+G(3df,2p)-S in the systems studied herein. The best result corresponds to the combination of the MPW1K functional with the 6-31++G(d,p) basis set complemented with the 6-311+G(3df,2p) for sulfur atom, that is, the 6-311+G(3df,2p)-S. The ratios obtained with this combination ($k_{1,2}/k_{1,1} = 2.4$ and $k_{1,3}/k_{1,1} = 23.7$) are in very good agreement with the corresponding experimental values, 1.3 and 24.4, respectively. The MP2 method also provides good results with this basis set, but the computational cost is not

Table 7. Deprotonation Energies for Monomers 1–8, Calculated at the MPW1K/6-311+G(3df,2p)-S//B3LYP/6-31+G(d,p) Level

monomer	ΔE (kJ/mol)	monomer	ΔE (kJ/mol)
1	1514	5	1482
2	1509	6	1528
3	1482	7	1530
4	1466	8	1483

comparable to that of the MPW1K functional. As a conclusion, the MPW1K/6-311+G(3df,2p)-S level is the most adequate for the calculation of rate coefficients of sulfur-containing systems, thanks to its high accuracy and relatively low computational cost.

The relative reactivity toward proton abstraction by a base can be estimated by calculating the deprotonation energies at the carbon position:

$$\Delta E = E(\text{anionic monomer}) + E(\text{H}^+) - E(\text{neutral monomer}) \quad (3)$$

Geometry optimizations of monomers 1–8 and the corresponding anions were carried out at the B3LYP/6-31+G(d,p) level of theory, and energy calculations on the optimized structures were subsequently computed with MPW1K/6-311+G(3df,2p)-S, following the conclusions described in the previous paragraph. The computed deprotonation energies are listed in Table 7. Despite the simplicity of the model considered, in which all calculations have been carried out in gas phase and without inclusion of the base or any stabilizing effect of the solvent, there is a very good correlation between the deprotonation energies predicted by the theoretical calculation and the relative formation rate of precursors (t_{max}) experimentally determined, as can be observed clearly in Figure 7, indicating that the choice of methodology is appropriate.

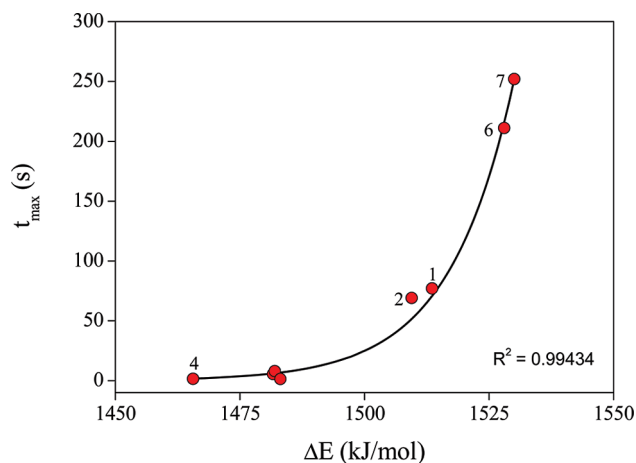


Figure 7. t_{\max} versus deprotonation energies for monomers 1–8.

Effect of Solvation on Mechanism and Kinetics. The high absolute values of computed rate coefficients at all levels of theory (Table 6) indicate that important effects of stabilization have not been taken into account in the simple gas-phase models described earlier. Interaction with the solvent, 2-butanol, is expected to provide stabilization to the global anionic system through hydrogen bonds between the negatively charged oxygen of the *tert*-butoxide and the alcoholic proton of surrounding solvent molecules.

In many theoretical studies, the solvent is either neglected or simulated by means of continuum solvation models,^{45–47} in which the solvent is represented as a continuous medium characterized by a static dielectric constant. When explicit solute-solvent interactions are not very significant, these results give the correct reactive behavior. However, in many cases, such interactions play an important role in the first solvation shell and dielectric models are not adequate to describe them. One alternative to tackle this problem is to include explicit solvent interactions by placing discrete solvent molecules around the chemically active species.^{33,48–55} The number of explicit solvent molecules to be incorporated is generally determined by the value at which the coordination solvation energy (CSE) converges.^{48–51} Moreover, bulk solvation effects can be taken into account by placing the supermolecule in a continuum with a fixed dielectric constant (mixed implicit/explicit solvent model).^{29–32} However, a recent study carried out by Warshel³² points out that mixed implicit/explicit solvation models do not always give reliable results, and are highly dependent on the number and orientation of explicit solvent molecules.

In the present study, the effect of solvation was modeled by explicitly including an optimum number of solvent molecules. The objective is to see the effect of solvent stabilization on reaction rate coefficients and to improve the correlation between experimental and calculated absolute rate constants. Because of the large size of the solvated system, only one monomer (monomer **2**) has been studied with the solvated cluster approach. It is important to note that these systems are inherently floppy due to the loose intermolecular interactions between solvent and solute molecules, and therefore, it is difficult to make a legitimate comparison between solvated systems, since the difference in position and alignment of solvent molecules may have a cumulative influence on energetics. Thus, the aim in applying this approach is to better reproduce experimental absolute rate constants rather than reproducing the relative ratios among monomers. Two simplifications have been made that are not expected to significantly influence the qualitative results. The

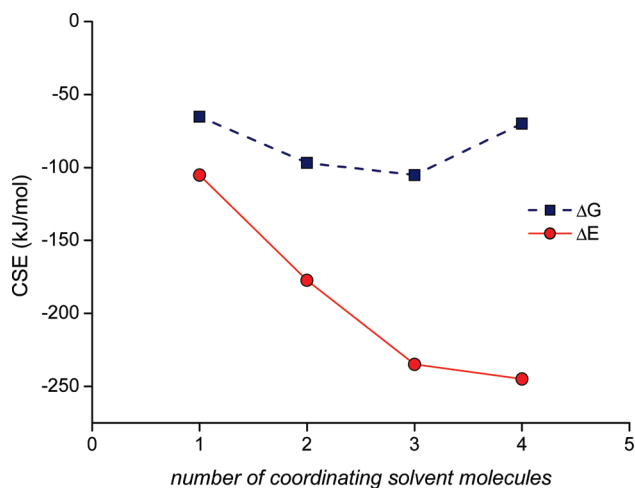


Figure 8. Coordination solvation energy (CSE) corresponding to the coordination of the *tert*-butoxide anion by a different number of solvent molecules.

first one is the reduction of the monomer side chain (octyl) to an ethyl group, and the second one is the consideration of methanol as solvent instead of 2-butanol.

The optimum coordination number was determined first by coordinating an increasing number of solvent molecules to the *tert*-butoxide anion and assessing the convergence in coordination solvation energy (Figure 8). As expected, the free energy of coordination converges faster than electronic energy due to the entropic effect of solvation. Coordination of the first two solvent molecules is highly exothermic (free CSE amount to -65.1 and -96.8 kJ/mol, respectively). The inclusion of a third molecule causes only a slight additional stabilization (-105.1 versus -96.8 kJ/mol), and no coordination effectiveness is found when four coordinating molecules are considered. As a conclusion, the adequate coordination number for the *tert*-butoxide is three. Taking into account that the anion has to abstract a hydrogen from the reactant, it is necessary to leave one free channel; therefore, two solvent molecules were coordinated to the base. It is important to note that, as discussed earlier in the paper, the abstraction of the proton is immediately (or simultaneously) followed by the expulsion of the leaving group, chloride in monomers **1** and **3**, and bromide in monomer **2**. Therefore, solvation of the halogen ion is expected to play an important role in this process. In order to treat the system more consistently, solvation of the leaving group and the sulfinyl group have been included. CSE convergence calculations, as described earlier, have shown that the required number of explicit solvent molecules for the halide and the sulfinyl oxygen is three and two, respectively. The overall number of methanol molecules included in the cluster calculations is seven, considerably increasing computational cost.

The supermolecule was built by coordinating solvent molecules onto the previously optimized gas-phase geometries and performing a new optimization of the solvated system. Afterward, internal reaction coordinate (IRC) calculations were performed in order to find the reactants and product structures that are connected by that transition state. The MPW1K/6-311+G(3df,2p)-S//B3LYP/6-31+G(d,p) electronic structure method was applied for calculations, following the conclusions described in the previous sections.

The optimized geometry of the solvated transition state corresponding to monomer **2** is depicted in Figure 9 (xyz coordinates and low frequency modes provided in the

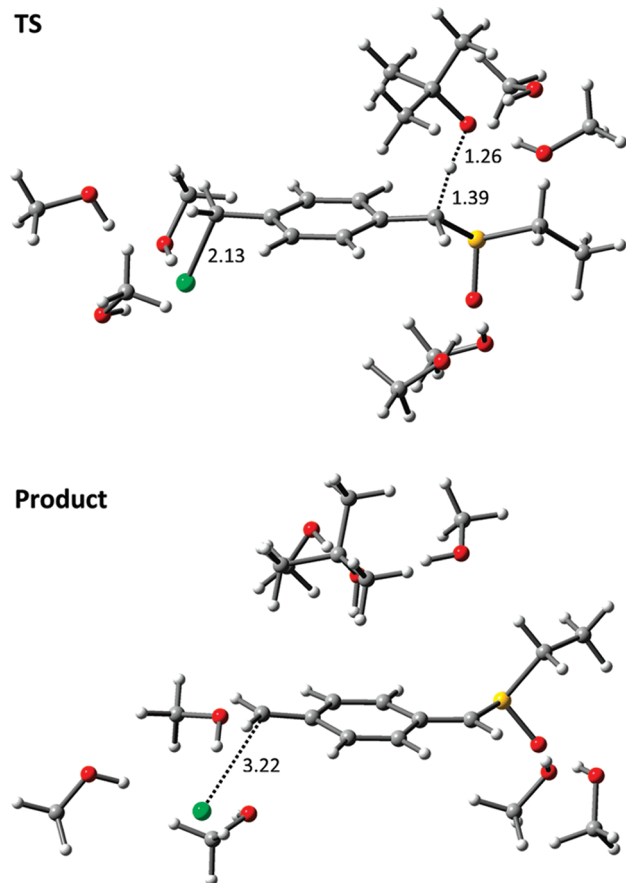


Figure 9. The solvated transition state (top) and product (bottom) corresponding to the reaction of monomer **2** with *tert*-butoxide, optimized at B3LYP/6-31+G(d,p). All distances in Å.

Supporting Information). It is interesting to compare critical distances with gas-phase results (Table 4). The length of the forming bond between the oxygen and the proton is shorter when solvent is included (1.26 versus 1.33 Å) whereas the breaking bond is longer (1.39 versus 1.31 Å). The elongation of the carbon–hydrogen bond and shortening of the new bond indicate that the transition state of the solvated system has a product-like structure; that is, it is a “late” transition state, which is usually characterized by higher barrier heights than “early” ones.

Kinetic parameters were calculated according to eq 1 similar to the gas phase section. The activation energy on the solvated system at the MPW1K/6-311+G(3df,2p)-*S* level of theory is 49.8 kJ/mol, around 4-fold the value predicted by gas-phase calculations, and the reaction rate coefficient is $1.41 \times 10^5 \text{ L mol}^{-1} \text{ s}^{-1}$, almost 5 orders of magnitude lower than that obtained in the absence of solvent. The stabilizing effect of solvation is very crucial, especially in the case of the *tert*-butoxide anion, which is very unstable in gas phase. This effect is greater in the reactant than in the transition state since in the latter the anion is partially stabilized by the proton that it is abstracting. As a consequence, the barrier is much higher when the solvent is included and the rate constant decreases several orders of magnitude. Although experimental rate coefficients are not yet matched by these calculations even with the explicit inclusion of the solvent, its effect on the kinetics of this reaction is clearly demonstrated. The difference may be ascribed to the simplifications made in the calculations, which were necessary due to large size of the system, since the consideration of the octyl side chain on the

monomer and 2-butanol as implicit solvent would make calculations unaffordable.

The product obtained from IRC calculations and subsequent reoptimization with B3LYP/6-31+G(d,p) has shown that an intermediate carbanion does not exist, but the final product of the reaction is the *p*-quinodimethane derivative, as can be seen in Figure 9. All attempts to locate the carbanion, including explicit solvation of the carbanion and MP2 optimizations on the solvent cluster, have failed, always resulting in simultaneous proton abstraction and expulsion of the leaving group. As clearly seen in Figure 9, the deprotonated carbon becomes planar and the bromine leaves. The driving force in the expulsion of the leaving group is most likely the extended conjugation in the final product. As indicated earlier, this effect was also partially observed in gas-phase calculations (Figure 6). In that case, although the carbon–halogen length is elongated with respect to the reactant (Table 4), the bare ion cannot completely leave due to the lack of a proper molecular environment, which is later provided in the solvated cluster calculations. This has already been reported for the Gilch route by Rehahn et al.,^{56,57} whose attempts to locate the carbanion failed, resulting in a spontaneous loss of the corresponding halide anion. It is clear that the inclusion of solvation in the modeling of this reaction is prominent to correctly reproduce this process and to state unequivocally the type of mechanism at play. Theoretical results clearly point toward a concerted E_2 mechanism rather than a E_{1cb} .

Conclusions

From the experimental viewpoint, it is concluded that *in situ* UV–vis spectroscopy is a powerful tool in providing kinetic evidence for the formation of *p*-quinodimethane systems in the sulfinyl precursor route for the polymerization of PPV being highly relevant for mechanistic assumptions. Both a qualitative and a quantitative study on eight different monomers with different polarizer and leaving groups afforded kinetic data that can be fitted using a nonlinear least-squares method.

Additionally, a theoretical modeling of the reaction has been carried out in order to gain insight into the mechanism. Rate coefficients have been estimated on the basis of the transition state theory, in which a variety of electronic structure methods were considered. The MPW1K functional with the 6-31++G(d,p) basis set complemented with the 6-311+G(3df,2p) for the sulfur atom has proved to be the most adequate level for the rate constant calculations of sulfur-containing systems. The qualitative trend of the rate coefficients was correctly reproduced by gas-phase calculations; however, computed absolute values were several orders of magnitude higher than the experimental ones. The inclusion of explicit solvent was shown to be crucial, since the solvent effect is of great importance in the stabilization of ionic species and, thus, in the prediction of the reaction barriers. The presence of the solvent has decreased rate constants around 5 orders of magnitude compared to gas-phase results, bringing them closer to the experimental data. Theoretical results indicate that a concerted E_2 mechanism is more likely for *p*-quinodimethane formation in the sulfinyl precursor route, which is also consistent with experimental evidence. This conclusion is very important for the further rationalization of the propagation reaction in the PPV polymerization, which could occur either through a radical or an anionic mechanism.

Acknowledgment. The BOF-UHasselt is acknowledged for PhD grants for F.M. This work is supported by the IAP-BELSP0 program in the frame of IAP 6/27. The Fund for Scientific Research Flanders (FWO) and the Research Board of Ghent

University are acknowledged for financial support. Computational resources and services used in this work were provided by Ghent University. L.H. thanks the Spanish Ministry of Education (Programa Nacional de Movilidad de Recursos Humanos del Plan Nacional de I-D+i 2008-2011) and the Spanish Science and Innovation Ministry (MAT2008-06725-C03-02) for financial support.

Supporting Information Available: Cartesian coordinates of B3LYP/6-31+G(d,p) optimized geometries of all reactants, transition states and products; imaginary and low frequency modes of transition states; the experimental setup of the UV-vis stop flow accessory. This material is available free of charge via the Internet at <http://pubs.acs.org>.

References and Notes

- (1) (a) Shirakawa, J.; Louis, E. J.; MacDiarmid, A. G.; Chiang, C. K.; Heeger, A. J. *J. Chem. Soc., Chem. Commun.* **1977**, 578. (b) Kraft, A.; Grimsdale, A. C.; Holmes, A. B. *Angew. Chem., Int. Ed.* **1998**, *37*, 403. (c) Thompson, B. C.; Fréchet, J. M. J. *Angew. Chem., Int. Ed.* **2008**, *47*, 58.
- (2) Burroughes, J. H.; Bradley, D. D. C.; Brown, A. R.; Marks, R. N.; Friend, R. H.; Holmes, A. B. *Nature* **1990**, *347*, 539.
- (3) Wessling, R. A. J. *Polym. Sci., Polym. Symp.* **1985**, *72*, 55.
- (4) Gilch, H. G.; Wheelwright, W. L. *J. Polym. Sci., Part A: Polym. Chem.* **1966**, *4*, 1337.
- (5) Louwet, F.; Vanderzande, D.; Gelan, J.; Mullens, J. *Macromolecules* **1995**, *28*, 1330.
- (6) Son, S.; Dodabalapur, A.; Lovinger, A. J.; Galvin, M. E. *Science* **1995**, *269*, 376.
- (7) (a) Henckens, A.; Duyssens, I.; Lutsen, L.; Vanderzande, D.; Cleij, T. J. *Polymer* **2006**, *47*, 123. (b) Vandenbergh, J.; Wouters, J.; Adriaenssens, P. J.; Mens, R.; Cleij, T. J.; Lutsen, L.; Vanderzande, D. J. M. *Macromolecules* **2009**, *42*, 3661.
- (8) (a) Cho, B. R.; Kim, Y. K.; Han, M. S. *Macromolecules* **1998**, *31*, 2098. (b) Cho, B. R.; Kim, T. H.; Kim, Y. K.; Kim, N. S. *Macromolecules* **1999**, *32*, 3583. (c) Cho, B. R.; Kim, T. H.; Son, K. H.; Kim, Y. K.; Lee, Y. K.; Jeon, S. J. *Macromolecules* **2000**, *33*, 8167.
- (9) Van Breemen, A. J. J. M.; Issaris, A. C. J.; de Kok, M. M.; Van Der Borgh, M. J. A. N.; Adriaenssens, P. J.; Gelan, J. M. J. V.; Vanderzande, D. J. M. *Macromolecules* **1999**, *32*, 5728.
- (10) Vanderzande, D.; Issaris, A.; Van Der Borgh, M.; van Breemen, A.; de Kok, M.; Gelan, J. *Macromol. Symp.* **1997**, *125*, 189.
- (11) (a) Gillissen, S. PhD Dissertation, LUC Diepenbeek, Belgium, 2002. (b) Gillissen, S.; Lutsen, L.; Vanderzande, D.; Gelan, J. *Synth. Met.* **2001**, *119*, 137.
- (12) Gaussian 03, Revision D.01: Frisch, M. J.; Trucks, G. W.; Schlegel, H. B.; Scuseria, G. E.; Robb, M. A.; Cheeseman, J. R.; Montgomery, J. A., Jr.; Vreven, T.; Kudin, K. N.; Burant, J. C.; Millam, J. M.; Iyengar, S. S.; Tomasi, J.; Barone, V. et al. Gaussian, Inc., Pittsburgh, PA, 2003.
- (13) Verstraelen, T.; Van Speybroeck, V.; Waroquier, M. *J. Chem. Inf. Model.* **2008**, *48* (7), 1530.
- (14) Becke, A. D. *J. Chem. Phys.* **1993**, *98*, 5648.
- (15) Lee, C. T.; Yang, W. T.; Parr, R. G. *Phys. Rev. B* **1988**, *37*, 785.
- (16) Qingping, L.; Hongbing, J. I.; Shushen, L. V. *Int. J. Quantum Chem.* **2009**, *109*, 448.
- (17) (a) Lynch, B. J.; Fast, P. L.; Harris, M.; Truhlar, D. G. *J. Phys. Chem. A* **2000**, *104*, 4811. (b) Lynch, B. J.; Zhao, Y.; Truhlar, D. G. *J. Phys. Chem. A* **2003**, *107*, 1384.
- (18) Becke, A. D. *J. Chem. Phys.* **1996**, *104*, 1040.
- (19) Adamo, C.; Barone, V. *J. Chem. Phys.* **1998**, *108*, 664.
- (20) Zhao, Y.; Truhlar, D. G. *J. Phys. Chem. A* **2004**, *108*, 6908.
- (21) Adamo, C.; Barone, V. *J. Chem. Phys.* **1999**, *110*, 6158.
- (22) Boese, A. D.; Martin, J. M. L. *J. Chem. Phys.* **2004**, *121*, 3405.
- (23) Moller, C.; Plesset, M. S. *Phys. Rev.* **1934**, *46*, 618.
- (24) Papajak, E.; Leverentz, H. R.; Zheng, J.; Truhlar, D. G. *J. Chem. Theory Comput.* **2009**, *5*, 1197.
- (25) Scott, A. P.; Radom, L. *J. Phys. Chem.* **1996**, *100*, 16502.
- (26) Kormos, B. L.; Cramer, C. J. *J. Phys. Org. Chem.* **2002**, *15*, 712.
- (27) (a) Wynne-Jones, W. F. K.; Eyring, H. J. *J. Chem. Phys.* **1936**, *3*, 492. (b) Evans, M. G.; Polanyi, M. *Trans. Faraday Soc.* **1935**, *31*, 875. (c) Evans, M. G.; Polanyi, M. *Trans. Faraday Soc.* **1937**, *33*, 448.
- (28) (a) Ghysels, A.; Verstraelen, T.; Hemelsoet, K.; Waroquier, M.; Van Speybroeck, V. *J. Chem. Inf. Model.*, **2010**, in revision. (b) <http://molmod.ugent.be/code/wiki/TAMkin>.
- (29) da Silva, E. F.; Svendsen, H. F.; Merz, K. M. *J. Phys. Chem. A* **2009**, *113*, 6404.
- (30) Kelly, C. P.; Cramer, C. J.; Truhlar, D. G. *J. Phys. Chem. A* **2006**, *110*, 2493.
- (31) Pliego, J. R.; Riveros, J. M. *J. Phys. Chem. A* **2001**, *105*, 7241.
- (32) Kamerlin, S. C. L.; Haranczyk, M.; Warshel, A. *ChemPhysChem* **2009**, *10*, 1125.
- (33) De Sterck, B.; Vaneerdeweg, R.; Du Prez, F.; Waroquier, M.; Van Speybroeck, V. *Macromolecules* **2010**, *43*, 827.
- (34) *Chemical Reactor Theory: An Introduction*; Denbigh, K. G., Turner, J. C. R., Eds.; Cambridge University Press: Great Britain, 1971; p 30.
- (35) Izgorodina, E. I.; Coote, M. L. *Chem. Phys.* **2006**, *324*, 96.
- (36) Yu, X. R.; Pfaendtner, J.; Broadbelt, L. J. *J. Phys. Chem. A* **2008**, *112*, 6772.
- (37) Van Cauter, K.; Van Speybroeck, V.; Waroquier, M. *ChemPhysChem* **2007**, *8*, 541.
- (38) Hemelsoet, K.; Van Durme, F.; Van Speybroeck, V.; Van Reyniers, M.-F.; Van Waroquier, M. *J. Phys. Chem. A* **2010**, *114*, 2864.
- (39) Hemelsoet, K.; Van Speybroeck, V.; Waroquier, M. *J. Phys. Chem. A* **2008**, *112*, 13566.
- (40) Bauschlicher, C. W., Jr.; Partridge, H. *Chem. Phys. Lett.* **1995**, *240*, 533.
- (41) (a) Bell, R. D.; Wilson, A. K. *Chem. Phys. Lett.* **2004**, *394*, 105. (b) Yockel, S.; Wilson, A. K. *Chem. Phys. Lett.* **2006**, *429*, 645.
- (42) Denis, P. A.; Ventura, O. N. *Chem. Phys. Lett.* **2001**, *344*, 221.
- (43) Stoffregen, S. A.; McCulla, R. D.; Wilson, R.; Cercone, S.; Miller, J.; Jenks, W. S. *J. Org. Chem.* **2007**, *72*, 8235.
- (44) Jiang, S.; Wang, Z.; Zhou, J.; Wen, Z.; Cen., K. *J. Zhejiang Univ., Sci., A* **2009**, *10* (9), 1327.
- (45) Cramer, C. J.; Truhlar, D. G. In *Solvent Effects and Chemical Reactivity*; Kluwer: Dordrecht, 1996; pp 1–80.
- (46) Tomasi, J.; Mennucci, B.; Cammi, R. *Chem. Rev.* **2005**, *105*, 2999.
- (47) Takano, Y.; Houk, K. N. *J. Chem. Theory Comput.* **2004**, *1*, 70.
- (48) D'hooghe, M.; Van Speybroeck, V.; Van Nieuwenhove, A.; Waroquier, M.; De Kimpe, N. *J. Org. Chem.* **2007**, *72*, 4733.
- (49) D'hooghe, M.; Van Speybroeck, V.; Waroquier, M.; De Kimpe, N. *Chem. Commun.* **2006**, 1554.
- (50) Catak, S.; D'hooghe, M.; De Kimpe, N.; Waroquier, M.; Van Speybroeck, V. *J. Org. Chem.* **2009**, *75*, 885.
- (51) Catak, S.; D'hooghe, M.; Verstraelen, T.; Hemelsoet, K.; Van Nieuwenhove, A.; Ha, H.; Waroquier, M.; De Kimpe, N.; Van Speybroeck, V. *J. Org. Chem.*, **2010**, *75* (13), 4530.
- (52) Catak, S.; Monard, G.; Aviyente, V.; Ruiz-Lopez, M. F. *J. Phys. Chem. A* **2006**, *110*, 8354.
- (53) Van Speybroeck, V.; Moonen, K.; Hemelsoet, K.; Stevens, C. V.; Waroquier, M. *J. Am. Chem. Soc.* **2006**, *128*, 8468.
- (54) Catak, S.; Monard, G.; Aviyente, V.; Ruiz-Lopez, M. F. *J. Phys. Chem. A* **2008**, *112*, 8752.
- (55) Catak, S.; Monard, G.; Aviyente, V.; Ruiz-Lopez, M. F. *J. Phys. Chem. A* **2009**, *113*, 1111.
- (56) Schwalm, T.; Wiesecke, J.; Immel, S.; Rehahn, M. *Macromolecules* **2007**, *40*, 8842.
- (57) Schwalm, T.; Wiesecke, J.; Immel, S.; Rehahn, M. *Macromol. Rapid Commun.* **2009**, *30*, 1295.